Developmental Cell
Article

Serum Response Factor Is Required for Sprouting Angiogenesis and Vascular Integrity

Claudio Areias Franco,[1,2] Mathias Mericskay,[1,2] Ara Parlakian,[1,2] Guillaume Gary-Bobo,[1,2] Jacqueline Gao-Li,[1,2] Denise Paulin,[2] Erika Gustafsson,[3] and Zhenlin Li[1,2,*]
[1]UPMC Univ Paris 06, UMR 7079, Physiology and Physiopathology, 75005 Paris, France
[2]CNRS, UMR 7079, 75005 Paris, France
[3]Department of Experimental Pathology, Lund University, SE 221 85 Lund, Sweden
*Correspondence: zhenli@ccr.jussieu.fr
DOI 10.1016/j.devcel.2008.07.019

SUMMARY

Serum response factor (SRF) is a transcription factor that controls the expression of cytoskeletal proteins and immediate early genes in different cell types. Here, we found that SRF expression is restricted to endothelial cells (ECs) of small vessels such as capillaries in the mouse embryo. EC-specific *Srf* deletion led to aneurysms and hemorrhages from 11.5 days of mouse development (E11.5) and lethality at E14.5. Mutant embryos presented a reduced capillary density and defects in EC migration, with fewer numbers of filopodia in tip cells and ECs showing defects in actin polymerization and intercellular junctions. We show that SRF is essential for the expression of VE-cadherin and β-actin in ECs both in vivo and in vitro. Moreover, knockdown of SRF in ECs impaired VEGF- and FGF-induced in vitro angiogenesis. Taken together, our results demonstrate that SRF plays an important role in sprouting angiogenesis and small vessel integrity in the mouse embryo.

INTRODUCTION

Embryonic development depends on the establishment of a functional network of blood vessels for the transport of oxygen, nutrients, signaling molecules, circulating cells, and metabolic waste products between tissues and organs. The malformation or dysfunction of this network contributes to the pathogenesis of many diseases (Carmeliet, 2005). Embryonic blood vasculature tree formation involves two fundamentally different processes. Initially, vasculogenesis gives rise to a primary vascular plexus through the differentiation of precursor cells named hemangioblasts. Subsequently, angiogenesis leads to the formation of a complex vascular tree of variably sized vessels through tight coordination of cell proliferation, differentiation, migration, matrix adhesion, and the recruitment of mural cells (Hanahan and Folkman, 1996; Risau, 1997). Various signaling molecules, such as VEGF, FGF, TGF-β, PDGF, angiopoietins, Dll4, ephrins, netrins, semaphorins, and slit, have proven crucial in vascular tree development (Adams and Alitalo, 2007; Eichmann et al., 2005; Torres-Vázquez et al., 2004). These signaling pathways elicit an array of biological effects and intracellular signaling events that mediate their function in endothelial cells (ECs). The ultimate downstream effectors of these signaling pathways are transcription factors. To date, no EC-specific transcription factors have been identified, and it has been suggested that a combination of several transcription factors, such as Hox, FoxO, Ets, and GATA family members, as well as Vezf-1, SCL/Tal1, and Hey1 and 2, control gene expression in ECs (Dejana et al., 2007). Serum response factor (SRF) is an ancient and evolutionarily conserved transcription factor of the MADS-box family that binds to a CArG box ($CC(A/T)_6GG$) found in the regulatory regions of multiple genes involved in cell growth, migration, cytoskeletal organization, energy metabolism, and myogenesis (Treisman, 1987; Sun et al., 2006). The regulation of such divergent processes by SRF relies on its ability to associate with different cell-type-specific and signaling-responsive accessory cofactors or transcription factors, such as members of the Ets, myocardin, and GATA families. In addition, SRF mediates the activity of cytokines like endothelin-1 and angiotensin II, growth factors including PDGF and TGF-β, and catecholamines (Chai and Tarnawski, 2002; Miano, 2003). Tarnawski's group demonstrated that VEGF induces SRF expression and nuclear translocation and increases SRF-binding activity to the CArG box in ECs in vitro through both Rho-Actin and MEK-ERK signaling pathways (Chai et al., 2004). In this context, SRF is a downstream mediator of VEGF signaling in ECs and is required for VEGF-induced angiogenesis.

Classical disruption of the *Srf* gene in mice leads to an early embryonic death with a defect in mesoderm formation (Arsenian et al., 1998). Using a conditional Cre/loxP gene inactivation system, we and other groups have demonstrated the crucial role of SRF during embryogenesis for differentiation and for maturation of cardiac and smooth muscle cells (SMCs) (Parlakian et al., 2004; Miano et al., 2004; Niu et al., 2005). The role of SRF in the developing vascular system is, however, unknown. In order to investigate this further, we used the transgenic mouse line Tie1-Cre (Gustafsson et al., 2001) to trigger the specific loss of SRF in ECs. Here, we show that SRF expression is restricted to ECs of small vessels in the mouse embryo, and that SRF is particularly important for the expression of β-actin and VE-cadherin in ECs. Inactivation of the *Srf* gene in embryonic ECs leads to a decrease in the number of branching points, alterations in tip cell morphology, and the disruption of EC junctions. These defects result in aneurysm and hemorrhage formation in small vessels found predominantly in the limb buds, head, and tail, which ultimately leads to embryonic lethality at E14.5. Our results suggest a crucial role for SRF in sprouting angiogenesis and in the maintenance of small vessel integrity.

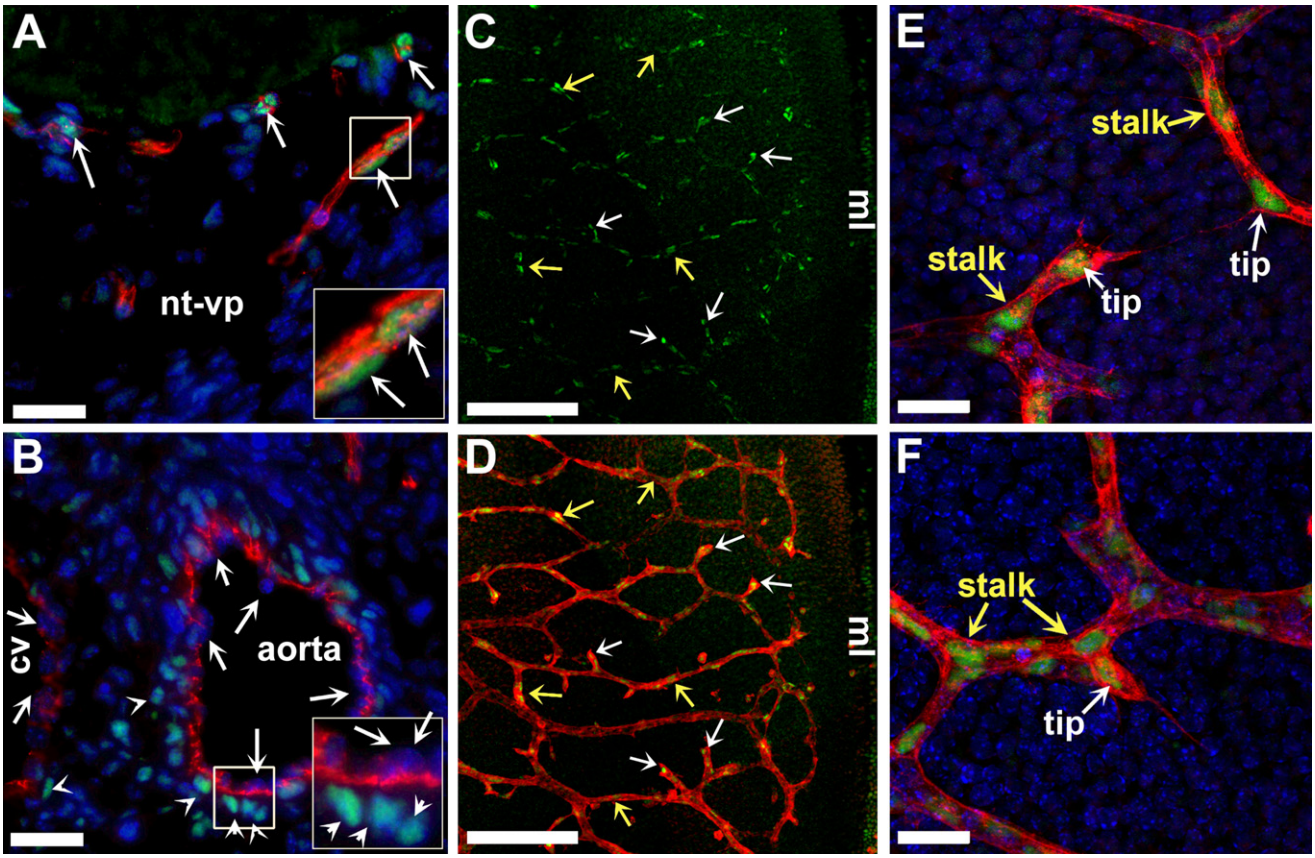

Figure 1. SRF Protein Is Detected Only in the ECs of Small Vessels in the Mouse Embryos

(A–F) Immunofluorescence images of anti-SRF antibodies (green), anti-PECAM1 (red) antibodies, and DAPI staining (blue) in E11.5 embryos. SRF is present in (A) ECs (arrows) of small vessels and the perineural vascular plexus, but not in (B) ECs of large vessels, like the aorta or cava vein. SMCs in the aorta are SRF positive (arrowheads). Inserts are a higher magnification of the regions indicated in (A) and (B). (C–F) Confocal images of hindbrain capillaries showing a strong expression of SRF in tip and stalk ECs of sprouting vessels. Tip cells are indicated by white arrows, and stalk cells are indicated by yellow arrows. (E and F) Higher magnification of sprouting capillaries. Cv, cava vein; nt-vp, neural tube vascular plexus. The scale bars are 25 μm in (A) and (B), 200 μm in (C) and (D), and 10 μm in (E) and (F).

RESULTS

ECs of Small Vessels Express SRF Protein in the Mouse Embryo

Using immunohistochemistry, we analyzed the expression of SRF in the vascular system of the mouse embryo (Figure 1). We found SRF expression in ECs of small vessels (diameter < 25 μm), the capillaries, arterioles, and venules (Figure 1A and data not shown), although not in ECs of large vessels (Figure 1B), such as the aorta and cava veins, in which SRF was only detected in SMCs. Interestingly, we observed SRF expression in both stalk and tip cells of sprouting capillaries, such as the hindbrain capillaries (Figures 1C–1F). This particular pattern of SRF protein expression suggests a specific role of SRF in the ECs of embryonic small vessels.

EC-Specific SRF Deletion Leads to Hemorrhage and Death at E14.5

To inactivate the *Srf* gene in ECs, we crossed SRF-floxed (abbreviated S^f/S^f) mice with the Tie1-Cre mice that express Cre in ECs as soon as E8.0 and in a minor population of hematopoietic cells (Gustafsson et al., 2001). The resulting $S^f/+$:Tie1-Cre double transgenic mice were viable. Intercrosses of $S^f/+$:Tie1-Cre males with S^f/S^f females (Figure 2A) yielded no S^f/S^f:Tie1-Cre pups (thereafter designated as SRF^{ECKO} or mutant) out of 151 viable offspring at birth. To determine when the SRF^{ECKO} embryos died, we examined litters from E8.5 to birth and obtained Mendelian ratios for the four possible genotypes (S^f/S^f, S^f/S^f:Tie1-Cre, $S^f/+$, and $S^f/+$:Tie1-Cre) between E8.5 and E13.5 (data not shown). PCR analysis from embryonic DNA indicated the deletion of the *Srf* gene as early as E8.5 (Figure 2B).

SRF^{ECKO} embryos from E8.5 to E10.5 were macroscopically indistinguishable from the control littermates (Figures 2C and 2D). Macroscopic examination revealed the presence of microhemorrhages and hematomas in the SRF^{ECKO} embryos that increased in size and number with age between E11.5 and E14.5. Large hematomas formed with high frequency at the limb buds, the tip of the tail, and the forebrain (arrows in Figure 2C). Extensive multifocal subcutaneous hemorrhages appeared at E13.5 and E14.5. Examination of histological sections revealed disrupted vessels with the diffusion of red blood cells

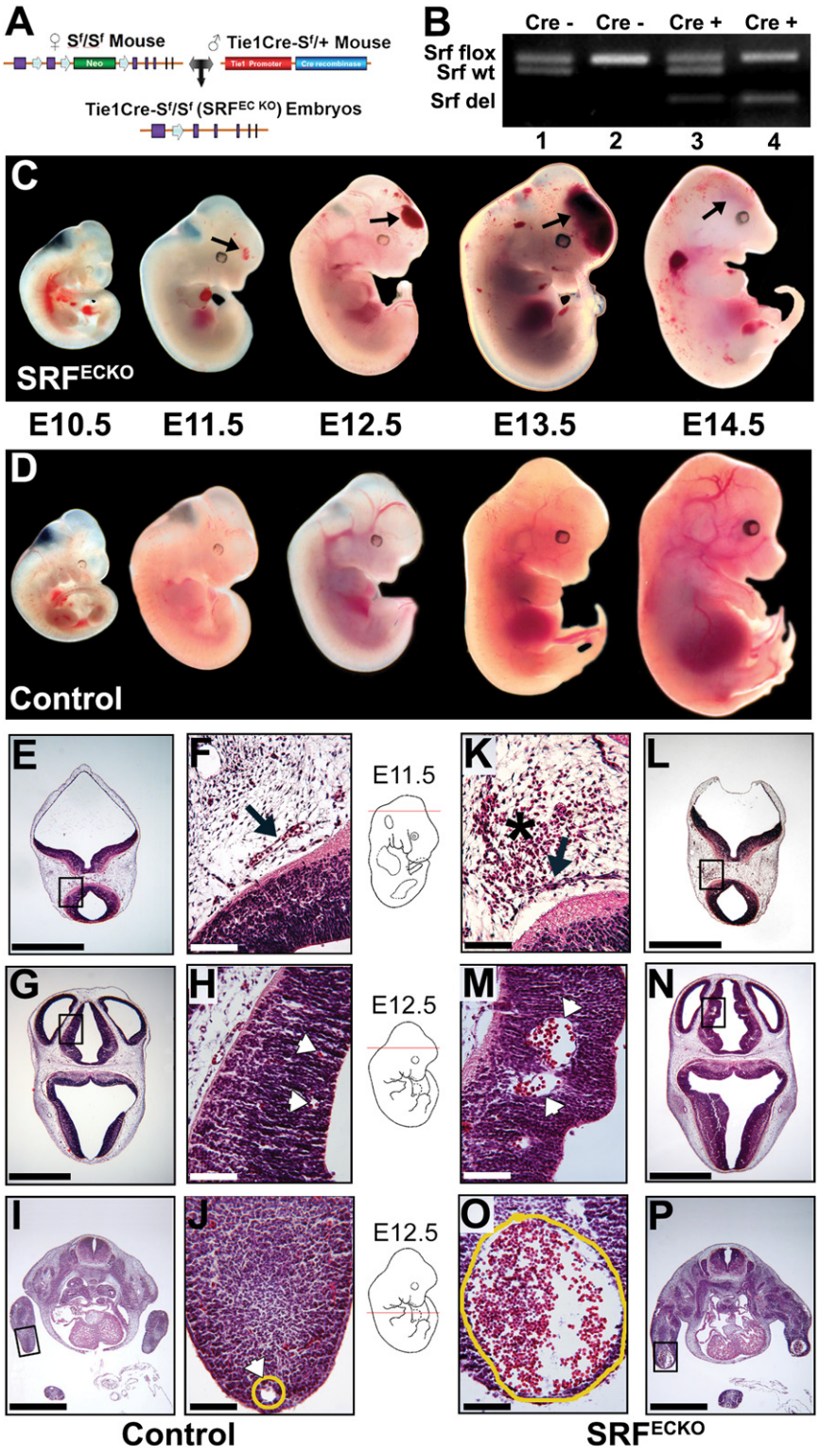

Figure 2. Tie1-Cre-Mediated Inactivation of SRF Leads to Capillary Aneurysms and Hemorrhages in the Mouse Embryo

(A) Schematic representation of Cre-mediated SRF exon 2 inactivation strategy.

(B) Genomic PCR analysis of the *Srf* gene on DNA of E8.5 embryos resulting from $S^f/+$:Tie1-Cre crossed with S^f/S^f. The four different genotypes ([1] $S^f/+$, [2] S^f/Sf, [3] $S^f/+$:Tie-Cre1, and [4] S^f/S^f :Tie-Cre1) were represented. The fragments corresponding to the floxed (flox), wild-type (wt), or deleted (del) exon 2 of the *Srf* gene are indicated.

(C and D) Whole-mount view of mutant and control embryos from E10.5 to E14.5. Hemorrhagic lesions in the forebrain region (arrows), limb buds, and tail were observed in E11.5 embryos.

(E–P) Histological analysis of (E–J) control and (K–P) mutant embryos. (F), (H), (J), (K), (M), and (O) are higher magnifications of the regions indicated in (E), (G), (I), (L), (N), and (P), respectively. Two types of vascular defects were observed in mutant embryos: (i) broken capillaries, as seen in the peri-neural vascular plexus (compare [K] and [L] to [E] and [F]), characterized by the (K and L) presence of blood cells (star) within mesenchyme; (ii) dilatation of vessels with the accumulation of red blood cells. Variable lumen enlargement of neural tube capillaries (compare [M] and [N] to [G] and [H]) and the extreme enlargement of the marginal vein in the limb bud (compare [O] and [P] to [I] and [J]) are presented.

The scale bars are 1 mm in (E), (G), (I), (L), and (N) and 100 μm in (P), (F), (H), (J), (K), (M), and (O).

into the perineural mesenchyme (Figure 2, compare [K] and [L] to [E] and [F]) and the subcutaneous capillaries (data not shown). We also observed extensive dilatations of intraneural capillaries, with or without endothelium rupture (Figure 2, compare [M] and [N] to [G] and [H]). The very large pouches of blood frequently observed in the limb buds were due to a dilatation of the marginal vein (Figure 2, compare [O] and [P] to [I] and [J]). This dilatation appeared secondary to malformations of the marginal vein. In fact, blood flow in the marginal vein of mutant embryos became bidirectional instead of unidirectional, as observed in controls (see Movies S1–S4 available online). Analysis of serial histological sections indicated an intact EC layer in most cases, thus suggesting a local dilatation of the vascular wall. We also found aneurysmal structures at the tip of the tail that are lined by a continuous endothelium (Figure 4G). A reduced rate of blood flow due to vessel malformations in the cephalic veins led to thrombus formation (Movie S5).

In agreement with the absence of SRF in the ECs of the aorta and cava vein, the formation and the stability of these vessels were not affected in SRF^{ECKO} embryos. We found no hemorrhagic or aneurysm defects in the extraembryonic vasculature of the mutant embryo (data not shown).

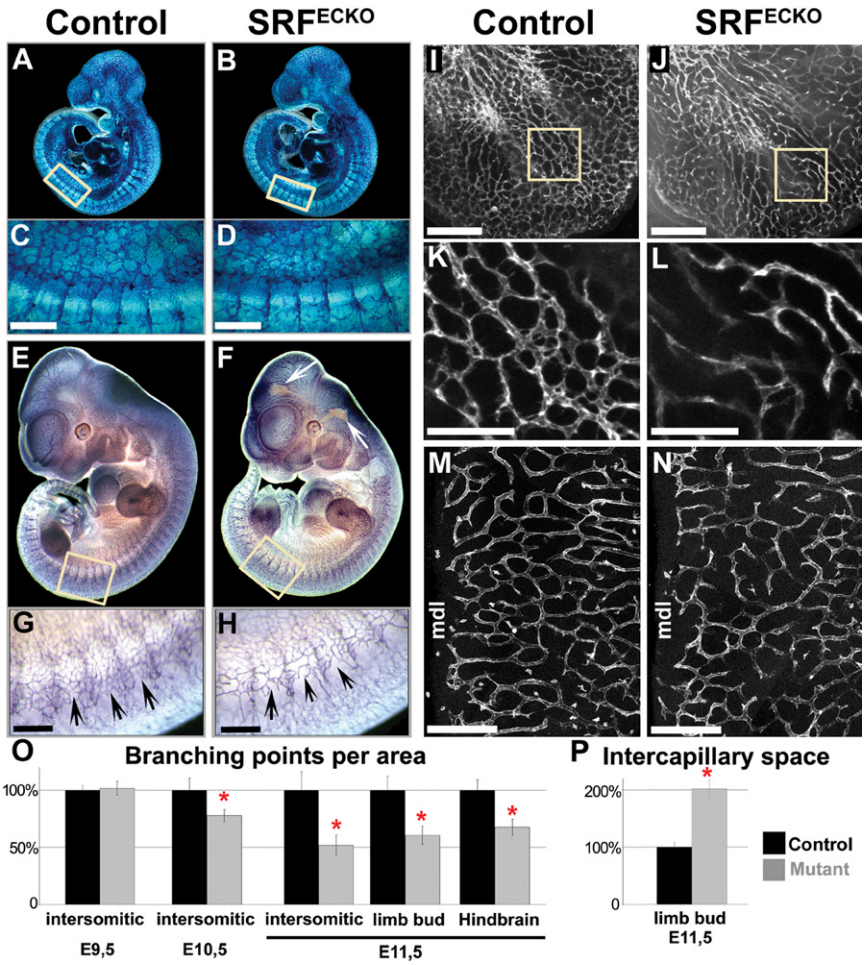

Figure 3. Reduced Vascular Capillary Network Density in SRF^{ECKO} Embryos

(A and B) Whole-mount view of X-gal staining of E9.5 (A) S^f/+:Tie1-Cre:R26/+ and (B) S^f/S^f :Tie1-Cre:R26/+ (mutant) triple transgenic embryos.

(C and D) Higher magnification of boxed regions in (A) and (B), respectively. We observed no obvious defect between mutant and control embryos at E9.5.

(E and F) Whole-mount immunohistochemical staining by anti-PECAM1 antibody on E11.5 embryos. Hemorrhagic lesions were indicated by arrows.

(G and H) Higher magnification of boxed regions in (E) and (F), respectively, show the reduction of vascular network density in the intersomitic region (arrows).

(I and J) Confocal immunofluorescence images of the (I) control and (J) mutant limb buds with anti-PECAM1 antibody on E11.5 embryos show similar branching reduction.

(K and L) Higher magnification of boxed regions in (I) and (J), respectively.

(M and N) Confocal images of hindbrain of E11.5 embryos labeled by isolectin B4 also show a reduced capillary density in mutant embryos. mdl, midline.

(O) Quantification of the number of branching points of the different regions at E9.5, E10.5, and E11.5. The data shown are means ± SEM. N = 6, *p < 0.05.

(P) Quantification of intercapillary space in limb buds of E11.5 control and mutant embryos. The data shown are means ± SEM. N = 6, *p < 0.05.

The scale bars are 250 μm in (C), (D), (G), (H), (I), (J), (M), and (N) and 100 μm in (K) and (L).

Reduced Vascular Branching and Increased Intercapillary Spaces in Mutant Embryos

In order to follow the fate of the ECs and compare the pattern of the vascular network in mutant and control embryos, we used the ROSA26 (R26) reporter line (Soriano, 1999). We crossed the S^f/+:Tie1-Cre males with homozygous S^f/S^f:R26/R26 females to generate S^f/+:Tie1-Cre:R26/+ (control) and S^f/S^f:Tie1-Cre:R26/+ (mutant) triple transgenic embryos. The E8.5 and E9.5 mutant embryos showed no obvious vascular defects, as indicated by the whole-mount X-gal coloration (Figures 3A–3D; Figure S1). However, a reduction in capillary density started at E10.5 and preceded the appearance of hemorrhagic lesions, arguing for a primary defect in sprouting angiogenesis in SRF^{ECKO} embryos. Whole-mount staining with an anti-PECAM1 antibody (Figures 3E–3H and 3I–3N) confirmed this observation. Quantification of the number of branching points in the intersomitic region of the trunk revealed a progressive decrease in the mutant starting at E10.5, reaching 50% that of controls by E11.5 (Figure 3O). Other regions of the embryo, such as the limb buds and hindbrain, also showed a similar decrease at this stage (Figures 3I–3O). Accordingly, the intercapillary area was larger in the mutant (Figure 3P). These results indicate a severely compromised capillary angiogenesis in SRF^{ECKO} embryos, whereas large vessels arising through vasculogenesis were unaffected.

Detailed Analysis of Angiogenic Defects and Aneurysm Formation in the Tail

Vessels in the tail form in a sequential and stereotypic manner that parallels the temporal order of somite formation, thus allowing a detailed analysis of the vascular defects. We observed the vascular network of the tail in S^f/+:Tie1-Cre:R26/+ control embryos at E11.5. As depicted in the schematic drawing (Figure 4A), the posterior ends of the paired caudal arteries connect to dorsolateral vessels that are themselves interconnected at the tip of the tail to form a half-circular tip vessel (also see Figure 4C). A dense capillary network branches out of the caudal vein, located ventral to the caudal artery, to join the dorsolateral vessels on each side of the tail (Figures 4A and 4B). In the SRF^{ECKO} embryos, however, we found a large decrease in the density of the capillary network joining the caudal vein to the dorsolateral vessel (Figure 4D), as well as irregularly shaped dorsolateral vessels that did not join at the tip of the tail (Figure 4E), but instead ballooned at the posterior end (stars, Figures 4D, 4E, 4G, and 4H). Whole-mount anti-PECAM1 staining of the tail at E12.5 showed the sizeable extent of this dilatation enclosing the ends of the caudal arteries and vein at this stage (Figure 4G). The intersomitic arteries branching from the caudal aorta developed normally in the SRF^{ECKO} embryo. In contrast, we found defects at the level of the secondary branches. The dorsolateral

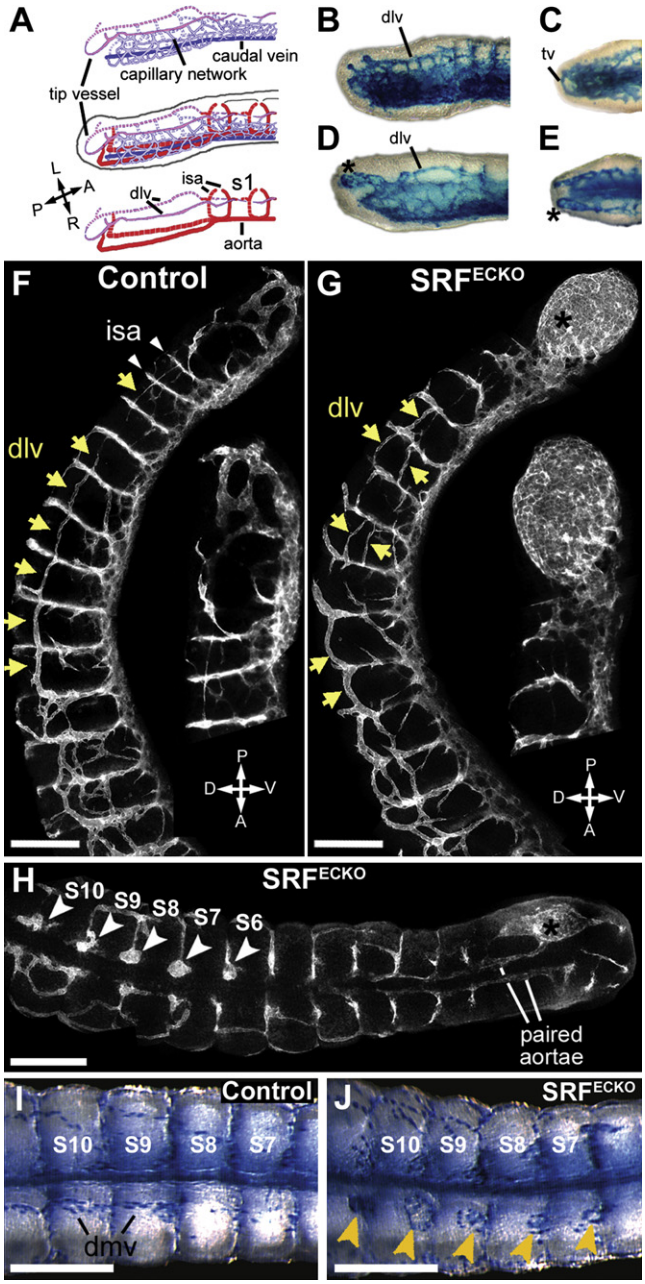

Figure 4. Aneurysm Formation Is Associated with Defective Sprouting Angiogenesis and Capillary Connections in the Tail

(A) Schematic drawing of vascular network development in the region near the tip of the tail (see Results section for details). Anterior-posterior (A-P) and left-right (L-R) axes are indicated.

(B–E) X-gal staining of E11.5 (B and C) S^f/+:Tie1-Cre:R26/+ and (D and E) S^f/S^f:Tie1-Cre:R26/+ triple transgenic embryos. We observed a reduction in capillary density of the dorsolateral vessels (dlv) and irregularly shaped dorsolateral vessels without the formation of a half-circular tip vessel (tv).

(F and G) Confocal images of the left lateral view of whole-mount immunofluorescence of E12.5 control and mutant embryo tails, with PECAM1 antibody. Defects were found at the level of the secondary branches in the mutant tail. Note the aneurysm-like dilation at the end of the caudal arteries and vein boundary region (star), as well as the anarchical connections of secondary branches of intersomitic vessels ([G], arrows), contrasting with the linear link of the dorsolateral vessels in control tail ([F], arrows).

(H) Confocal microscope image of PECAM1 immunostaining in the E12.5 mutant embryo confirmed the presence of aneurysm-like structures at the tail tip (star) and at the tips of intersomitic arteries (arrowheads).

(I and J) X-gal staining of the E12.5 triple transgenic embryos (I) S^f/+:Tie1-Cre:Vim-nls-lacZ and (J) S^f/S^f:Tie1-Cre:Vim-nls-lacZ (mutant). The nuclei of ECs are marked in blue. The aneurysm-like defects are observed once more and seemed to be time dependent (arrowheads in [J]). These defects were only observed in five formed somites (n° 6–10). The last forming somite near the tail tip is designated number 1 in (H)–(J). No real connection of dorsomedial vessels (dmv) between neighboring somites was observed in the region containing aneurysm-like defects.

The scale bars are 250 μm.

branches of the mutant were misaligned and discontinuous (Figure 4G) compared to the linear vessel formation found in the control (Figure 4F). In addition, the dorsomedial vessels connecting the dorsal ends of the intersomitic arteries on either side of the neural tube also showed defects in the mutant embryos. In controls, these vessels arise by sprouting angiogenesis, beginning at the level of somites 6–7 (the last forming somite near the tail tip is designated as number 1) and connecting over somite 8 (Figure 4I). In the mutants, we instead observed PECAM1-positive pouches at the dorsal end of the intersomitic arteries (Figure 4H, arrowheads). Using the Vim-nls-lacZ transgene (Colucci-Guyon et al., 1994) to label EC nuclei, we confirmed that the pouches were covered by ECs in mutant embryos (Figure 4J, arrowheads). Our observations suggest that the lack of SRF in ECs impairs sprouting angiogenesis at the tip of small vessels, thereby locally altering the connections between arteries and veins. Blood circulation is likely impaired in such a deficient network, and the tips of vessels are more prone to dilatation.

Altered EC-Specific Gene Expression in the Mutant Embryos

To investigate the consequence of targeted SRF inactivation on EC gene expression, we performed a real-time RT-PCR screen on a set of 41 genes mainly involved in EC functions (Figure 5A). RNA was extracted from limb buds of mutant and control embryos of the same litter. At E12.5, we found a 28% reduction of *Srf* mRNA in the mutant limb buds. This relatively low SRF reduction can be explained by the presence of other cells expressing SRF in the samples, such as muscle, mesenchymal, and epithelial cells. We found 21 significantly downregulated genes in the mutant. The transcriptional regulators *Creb1* and *Hdac7a* showed a 30%–40% reduction, whereas that of *c-fos* and *Vezf1* was not significant. We found a significant downregulation of *β-actin*, but not for muscle-specific genes such as smooth muscle *α-actin* and *desmin*. The aneurysms and microhemorrhages in histological sections prompted us to look at the expression of proteins involved in cell-cell and cell-matrix interactions in the SRF^{ECKO}. Mutants showed a 30% decrease in the mRNA level of genes encoding junctional proteins, such as *VE-cadherin*, *ZO-1*, and *occludin*, as well as *β1-*, *α1-*, and *α5-integrins*, whereas the expression level of *Pecam1* and *ZO-3* was unchanged. We examined the expression of several genes encoding proteins involved in signaling pathways in ECs. The expression level of *Alk1*, *Alk5*, *endoglin*, *angiopoietins 1* and *2*, *Vegfb*, *Vegfr2*, *Pdgfb*, and *Pdgfrb* was significantly decreased. Expression levels of *Tgfβ1*, *Tgfbr2*, *Tie2*, *Vegfa*, *Vegfr1*, *Pdgfa*, *Edg1*, and *Edg5* showed no significant change. The expression of

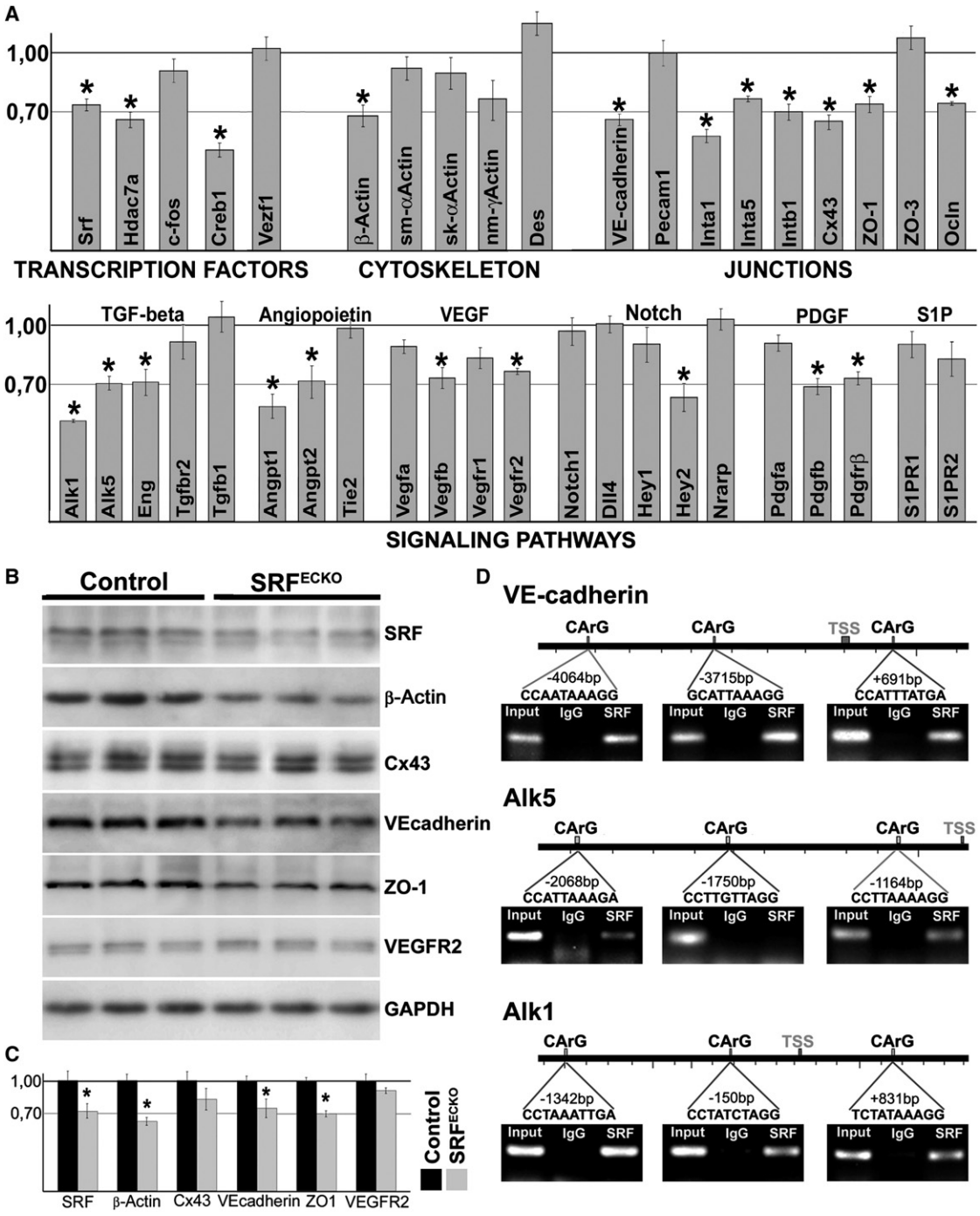

Figure 5. Altered Gene Expression in SRF^{ECKO} Embryos

(A) Quantification of mRNA levels in limb buds of E12.5 embryos by semiquantitative RT-PCR. All genes are normalized to *GAPDH*. The RNA level obtained for control limb buds was set to 1, and the ratios of mutant versus control limb buds is presented for each gene. The error bars represent SEM; N = 5, (*): $p < 0.05$ Student test.

(B) Western blot analysis of E12.5 embryo limb buds. Representative western blot analysis of control and mutant embryos is presented.

(C) The relative protein level of mutant versus control is presented. The level of control samples was set to 1. The error bars represent SEM; N = 6, (*): $p < 0.05$ Student test.

(D) ChIP analysis of SRF binding to murine genomic *VE-cadherin*, *Alk1*, and *Alk5* CArG elements in ECs. The sequences and positions of the putative SRF-binding sites found in the promoters and the downstream transcription start site (TSS) are indicated.

genes implicated in the Notch signaling pathway in ECs, such as *Notch1*, *Dll4*, and *Nrarp1*, were not affected, with the exception of *Hey2*, which was downregulated. We obtained similar results with RNA from the head (data not shown). Western blot analysis showed a 25%–30% reduction in protein levels for SRF, VE-cadherin, β-actin, and ZO-1 in the mutant limb buds at E12.5, in agreement with the decreased expression level of corresponding mRNAs (Figures 5B and 5C). Other proteins, such as VEGFR2 and connexin-43, showed no significant decrease.

Although *β-actin* is a known target of SRF, it is expressed in all cell types. Whether SRF controls EC-specific gene expression remains unresolved. On analyzing the promoter region (−5 kb to +1 kb) of the 21 downregulated genes, we found 18 presenting conserved CArG boxes between mouse and rat or mouse and human sequences (Table S1). Nine of the 21 had already been identified as SRF targets in previous studies on other tissues (Sun et al., 2006), and 12, including *VE-cadherin*, *Alk1*, *Alk5*, *endoglin*, and *Vegfr2*, represent potential new SRF targets in ECs. Chromatin immunoprecipitation (ChIP) experiments were performed in immortalized mouse brain ECs by using an SRF antibody. Interestingly, we found that SRF can bind to the three CArG boxes identified at the proximity of the *VE-cadherin* transcription start site (Figure 5D). We also found SRF interaction on putative CArG boxes for three other tested genes (*Alk1*, *Alk5*, and *endoglin*, Figure 5D; data not shown). In order to investigate a potential role of these CArG boxes in VE-cadherin expression, we inserted a 700 bp fragment containing two CArG boxes (−4064 and −3715) upstream of the 2.2 kb VE-cadherin promoter linked to luciferase. Analysis of luciferase activity indicated that mutation of the CArG box at −4064 significantly reduced the luciferase activity (Figure S2). In addition, we observed that the CArG boxes were needed for the promoter response toward VEGF and FGF. Our results suggest that *VE-cadherin* is a direct target of SRF in ECs.

Decreased Filopodia Number and Alteration in Filamentous Actin Organization of Endothelial Tip Cells in SRF^{ECKO} Embryos

The defects observed at the tip of sprouting vessels in mutant embryos prompted us to investigate the endothelial tip cells. Endothelial tip cell functions are tightly linked to the cytoskeleton dynamics. Our RT-PCR and western blot analyses showed a downregulation of β-actin in SRF^{ECKO} embryos. To visualize the actin cytoskeleton in tip cells, we focused our analysis on neural capillary sprouting given that the surrounding neural cells express low-level actin compared to mesenchymal cells in other regions of the embryo. We performed whole-mount immunostaining in the isolated hindbrain region of E11.5 embryos, by using isolectin B4 and phalloidin to label ECs and F-actin, respectively (Figure 6; Movies S6–S12). There was a clear reduction in the phalloidin signal at the level of the cortical actin underlying the EC membrane in both stalk (Figures 6B and 6D, arrows) and tip cells (Figures 6F and 6H, arrowheads). Aggregates of phalloidin-labeled F-actin were often observed at the base of filopodia extensions in the mutant tip cells (Figure 6H). Although the number of tip cells showed no change in SRF^{ECKO} embryos (control: 21.13 ± 3.49 tip cells/mm^2; mutant: 19.54 ± 3.89 tip cells/mm^2; n = 60, p = 0.626), we did observe a significant decrease in the number of filopodia extensions per tip cell (control: 6.56 ± 0.39; mutant: 4.98 ± 0.38; n = 72, p = 0.001). These filopodia also appeared thinner and less ramified (Figure 6G). Interestingly, vessel tips displayed a ballooned morphology in the SRF^{ECKO} mutant, with several stalk cells accumulating behind the tip cells (Figures 6C and 6G, stars) instead of the thin and straight vessels in controls (Figures 6A and 6E). Furthermore, we could detect more severe dilatations of the tip of some capillaries, which probably led to the aneurysmal structures observed in older stages of development (Movies S7 and S10). Our in vivo results could raise the question of whether SRF is more important for tip cell function or stalk cell function. To address this question, we used the aortic ring explant assay (Figures 6S–6X). We found that aortic rings explanted from S^f/S^f mice that were infected by the Cre-GFP adenovirus presented a mosaic inactivation of SRF in ECs. The observation of GFP labeling indicated that SRF-deficient cells could be recruited both as tip cells or stalk cells at the early time points. However, in both cases, the cells lacking SRF did not move over time and were either excluded from the sprouts or formed dilated glomerular structures at the tip of the sprout that were similar to the altered vessel tips observed in vivo (Figures 6S–6X). Infection with control GFP adenovirus did not alter the movements or the inclusion of the infected cells in the sprouts (data not shown).

Disrupted Interendothelial Junctions in Mutant Embryos

RT-PCR and western blot analyses showed the downregulation of several cell-cell junction proteins, including VE-cadherin and ZO-1. ZO-1 and VE-cadherin immunostaining of neural tube capillaries was reduced and showed a diffuse and dot-like pattern in SRF^{ECKO} capillaries, in contrast to the linear pattern observed in control EC membranes (Figure 6, compare [J] and [L] to [I] and [K], arrowheads). However, we observed no changes in VE-cadherin or ZO-1 staining in large vessels, including the carotid and the aorta (data not shown). In addition, we observed no difference in PECAM1 localization and immunofluorescence intensity levels between the control and mutant ECs of large and small vessels (Figures 3 and 4), in agreement with the normal expression levels of *Pecam1* measured by RT-PCR. Electron microscopy analysis of mutant and control E12.5 limb bud sections confirmed the alteration of interendothelial cell junctions, with shorter complexes compared to control vessels (Figures 6M–6R). We also detected a decrease in the number of adherens and tight junctions in mutant compared to control embryos, with a reduced electronic density at the level of the adherens junctions (arrows), suggesting a potential decrease in protein concentration in these regions. Moreover, large gaps could be observed (Figure 6N, asterisk) between the membranes of ECs, compared to the tight attachment seen in the control sections at this stage of embryogenesis (Figure 6M). Altogether, our results suggest a modification of EC junctions in the small vessels of SRF^{ECKO} mutant embryos.

siRNA-Mediated Knockdown of SRF Impairs VEGF- and FGF-Induced VE-Cadherin Expression, ERK1/2 Phosphorylation, and In Vitro Angiogenesis

To further characterize the role of SRF in EC biology, we knocked down SRF by using a small interfering RNA (siRNA) in primary human dermal microvascular ECs (HDMECs) and immortalized human bone morrow ECs (HUBMECs). siRNA treatment led to

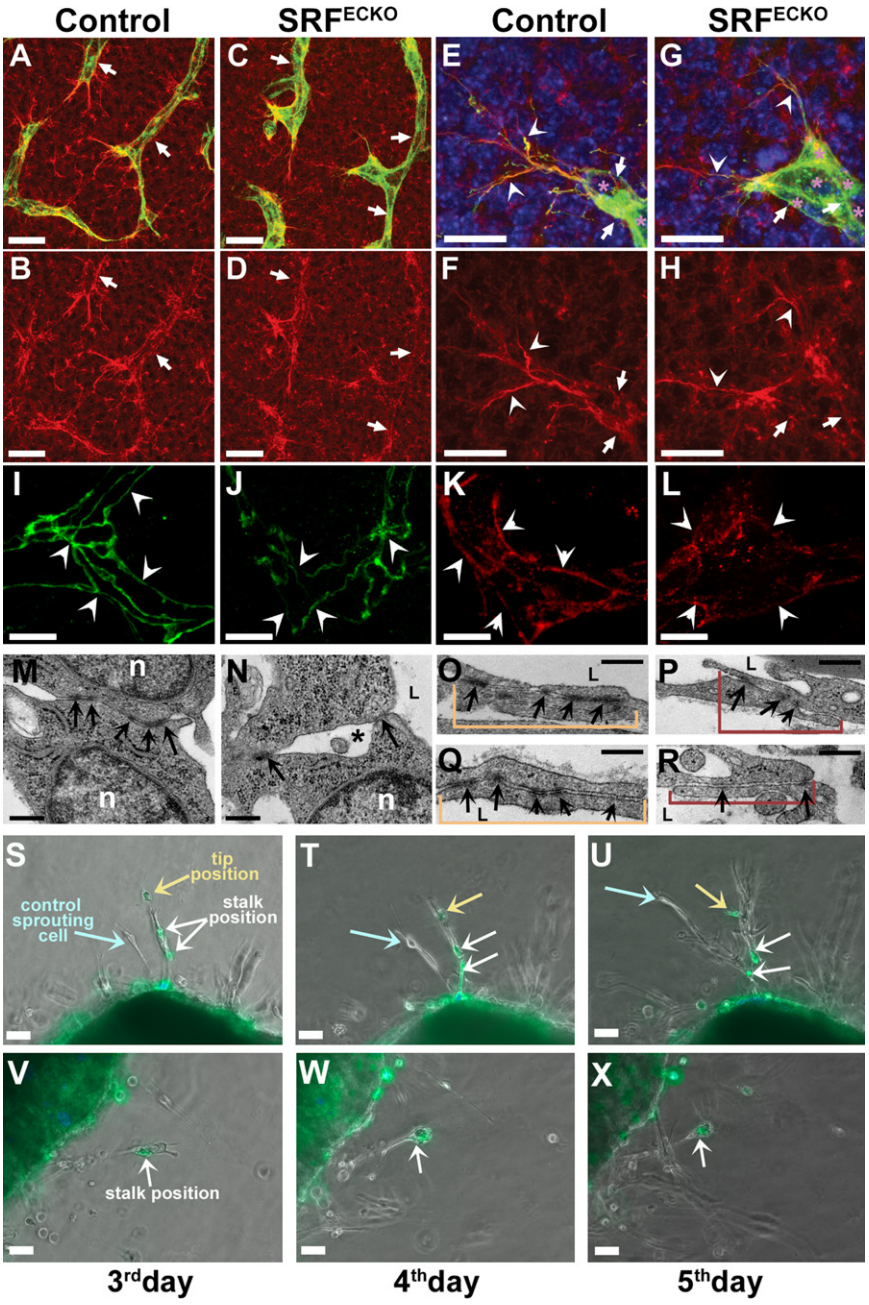

Figure 6. Alterations in Filamentous Actin Organization and Tip Cell Morphology in SRF^{ECKO} Embryos

(A–H) Confocal Z-stack projections of hindbrain capillaries of E11.5 (A, B, E, and F) control and (C, D, G, and H) mutant embryos. The hindbrains were stained by isoletinB4 (ECs, green) and phalloidin (F-actin, red). In the mutant hindbrain capillary, the intensity of F-actin staining was decreased, and the cortical actin cytoskeleton presents as a diffuse and dot-like structure, revealing an alteration in the actin cytoskeleton. The intensity of F-actin labeling in the filopodia extension (arrowheads) of tip cells was reduced in mutant embryos. (E and F) In control embryos, tip cells are at the edge of a monocellular linear structure. In mutants, however, the endothelial tip cells have a balloon-like morphology, (G and H) with an increased number of cells below the filopodia-protruding cell, as revealed by the DAPI-stained nuclei indicated by stars.

(I–L) Confocal images of (I and J) ZO-1 and (K and L) VE-cadherin immunofluorescence of control and mutant neural tube capillaries at E11.5. Compared to (I and K) control capillaries, ZO-1 and VE-cadherin labeling of (J and L) mutants was diffuse and localized in dot-like structures (arrowheads), suggesting an alteration in interendothelial junctions.

(M–R) Electron microscopy micrographs of (M, O, and Q) control and (N, P, and R) mutant limb bud capillaries at E12.5. The interendothelial junctions frequently showed shorter lengths (bracketed regions) in mutant embryos. We observed a decrease in the number of junctional complexes with a reduced density (arrows), as well as the occurrence of holes between ECs (asterisk) in some capillaries of mutant embryos. N, nuclei; l, lumen of the vessels.

(S–X) Aortic ring assay. Microscopic pictures of sprouting vessels from aortic ring explants of S^f/S^f mice infected with Ad-Cre-GFP virus, in Matrigel. (S–U) In different experiments, we could observe that SRF-deleted cells (GFP-expressing cells; green cells) were found both in the tip or stalk position within the sprouting vessel alongside control cells. However, the growth of the sprouts containing GFP-positive cells was impaired compared to control vessels in areas containing no SRF-deleted cell. This result suggests that the SRF-deficient cells can be recruited to sprout either as tip or stalk cells. However, the SRF-deficient cells compromise the normal migration of the vessel, even if the SRF-deficient cell is in a stalk position. (V–X) Moreover, when only one GFP-positive cell is in the stalk position, the defective expression of SRF leads to vessel growth arrest and an accumulation of cells in a glomerular form.

The scale bars are 10 μm in (A)–(D), 300 nm in (E)–(J), 25 μm in (I)–(L), 10 μm in (M)–(R), and 10 μm in (S)–(X).

a 80% decrease of *Srf* RNA and a 60% reduction of SRF protein (Figures 7A–7C). Immunofluorescence with an anti-SRF antibody confirmed a total of ~80% of cells without SRF staining (Figure S3). VEGF165 treatment significantly stimulated the SRF expression in these ECs (Figures 7A–7F and data not shown). The *Srf* mRNA level rapidly increased, reaching a maximum 30 min after VEGF treatment (Figure 7A). The SRF protein level also increased, reaching a maximum 2 hr after stimulation (Figures 7B and 7C). A luciferase reporter assay in ECs revealed that two CArG boxes, located in the 5′ proximal region of the SRF promoter, were needed for VEGF- or FGF-induced SRF expression (Figure S4). Deletion or mutation of these sites severely decreased the luciferase activity in both the basal condition and in VEGF- or FGF-stimulated cells.

Furthermore, we found a similar pattern of VE-cadherin expression and SRF expression at both the mRNA and protein levels in response to VEGF (Figures 7A–7C). We obtained similar results when cells were treated with bFGF (Figure S5). The *Srf*

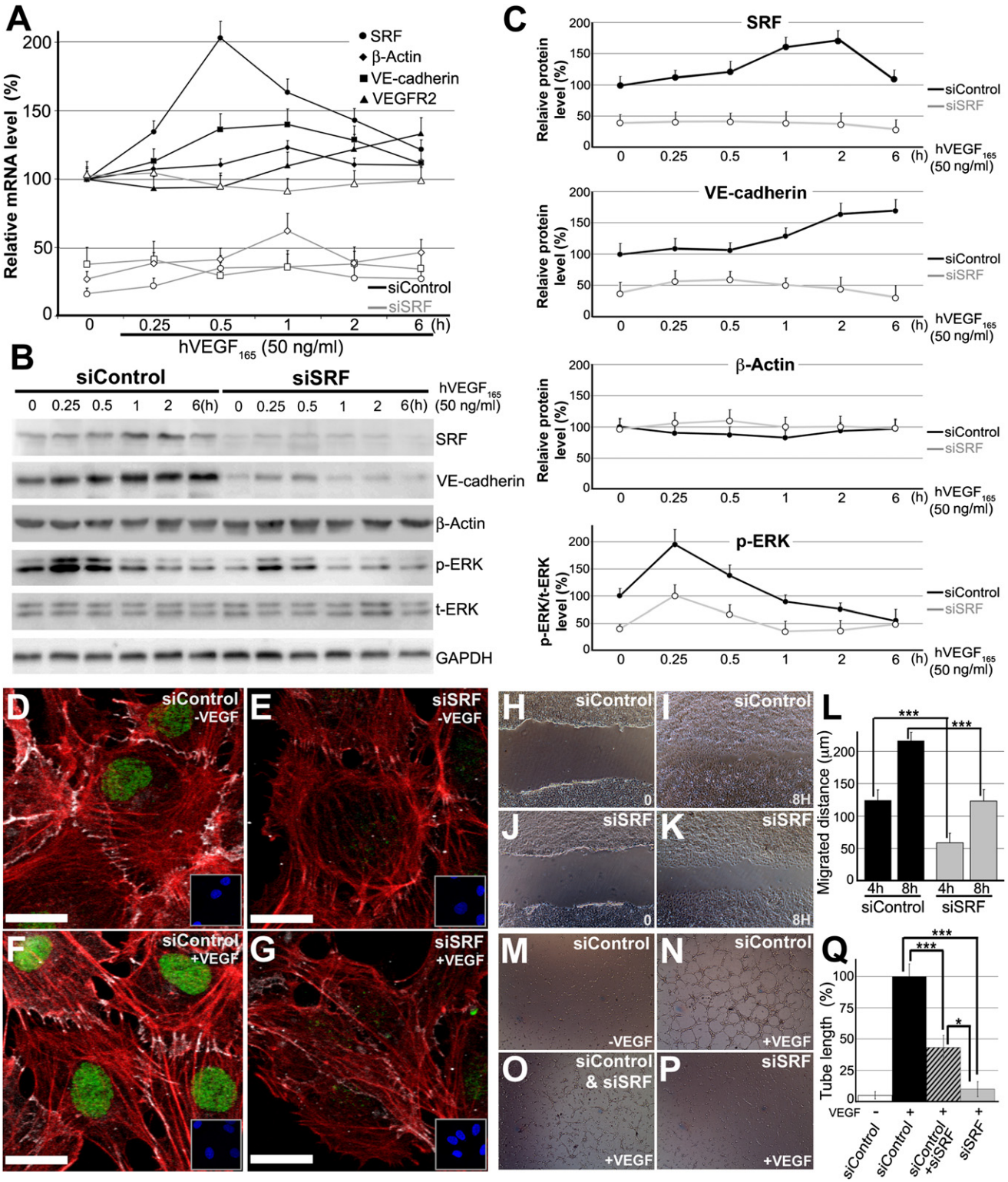

Figure 7. SRF Knockdown Impairs VEGF-Induced VE-Cadherin Expression, ERK1/2 Phosphorylation, and In Vitro Angiogenesis

(A) Quantification of relative mRNA levels of *Srf*, *VE-cadherin*, *β-actin*, and *VEGFR2* in VEGF-stimulated HDMECs treated with scrambled siRNA (siControl, black line) or siRNA against SRF (siSRF, gray line). The error bars represent SEM; N = 4.

(B) Representative western blot analysis of SRF, VE-cadherin, β-actin, phospho-ERK (p-ERK), and total-ERK (t-ERK) from VEGF-stimulated HDMECs treated with scrambled siRNA or *Srf* siRNA.

(C) Quantification of the relative protein levels of SRF, VE-cadherin, β-actin, and p-ERK/t-ERK. The error bars represent SEM; N = 3.

siRNA treatment led to a decrease in the expression of *VE-cadherin* and *β-actin* at the mRNA level, in correlation with the in vivo data (Figure 7A). The western blot data reveal a significant change in the VE-cadherin protein level, but not for β-actin, possibly due to its high stability (Figures 7B and 7C). Activation of SRF in ECs by VEGF has previously been shown to require ERK signaling (Chai et al., 2004). Interestingly, knockdown of the SRF protein level led to a decrease in MAPK/ERK1/2 phosphorylation in both basal and VEGF- or FGF-stimulated conditions (Figures 7B and 7C; Figure S5).

Immunofluorescence analysis indicated a decreased labeling of VE-cadherin and F-actin in ECs lacking SRF (Figure 7). Furthermore, we observed that VEGF stimulation increased the nuclear level of SRF and actin stress fibers (Figure 7F). These results demonstrate the importance of SRF in actin expression and dynamics, as well as VE-cadherin expression in ECs. Knockdown of SRF in ECs decreased cell migration (Figures 7H–7L) and inhibited the formation of tube-like structures in a Matrigel angiogenesis assay (Figures 7M–7Q). To address the question of whether SRF-deficient cells can be rescued by the presence of wild-type cells to incorporate tubular structures, we mixed control and SRF-depleted cells (1:1) prior to culture in Matrigel. The quantification of the total tube length of the mixed culture was less than 50% of the control tube length (Figures 7O and 7Q). Moreover, more than 90% of the cells in the tubular structures were derived from the control culture, as assessed by the detection of the fluorescent-labeled, scrambled siRNA (data not shown). These results show that the SRF-deficient cells have a cell-autonomous defect that prevents them from integrating tubular structures in vitro.

DISCUSSION

Our results reveal a key role of SRF in the angiogenic process and the maintenance of vascular integrity. Here, we have revealed that at early embryonic stages, SRF expression in ECs is restricted to vessels of small diameter: the capillaries, arterioles, and venules. Interestingly, we observed that both stalk and tip cells strongly express SRF, indicating an important role in sprouting angiogenesis. In SRF^{ECKO} embryos, we observed no obvious defects in vasculogenesis. Nor did we find an alteration in the early steps of angiogenesis that proceed from the remodeling of a pre-existing capillary plexus up to E10 in SRF^{ECKO} embryos. However, loss of the floxed *Srf* allele in ECs resulted in a decreased capillary density, the formation of aneurysmal structures in different regions, and, ultimately, multifocal hemorrhages and death around E14.5. Thus, SRF is important for sprouting angiogenesis and small vessel integrity in the mouse embryo.

The Control of Actin and VE-Cadherin Expression by SRF Is Essential in Sprouting Angiogenesis

One of the hallmarks of SRF^{ECKO} embryos is the important reduction in the number of branching points and capillary density. This reduction of the network complexity is often linked to defects in endothelial tip cell specification and migratory properties. In vertebrates, endothelial tip cells are located at the growing end of the capillary sprout, lack a lumen, and extend numerous long filopodia to explore growth factor signals and guidance cues in the surrounding tissue (Gerhardt et al., 2003). Tip cell fate is regulated in part by the Notch pathways that function as a negative feedback mechanism to ensure appropriate vessel patterning and prevent excessive vessel sprouting (Roca and Adams, 2007; Gridley, 2007). Deletion of Notch ligand Dll4 or Notch1 leads to an increase of tip cells and capillary density (Suchting et al., 2007; Hellström et al., 2007). In contrast, in SRF^{ECKO} mutants, no change in tip cell number and Notch1 or Dll4 expression were observed (Figure 5). Thus, SRF seems dispensable for tip cell fate.

The whole-mount phalloidin staining of F-actin in neural and tail capillaries revealed an altered organization of the actin cytoskeleton in ECs (Figure 6; Movies S6–S12). The tip cells of the SRF^{ECKO} embryos showed thinner and less numerous filopodia compared to control, with a spotty phalloidin signal at the base of the filopodia, suggesting a disorganized actin cytoskeleton in this region. Interestingly, this defect was found not only in tip cells, but also in stalk cells. In addition, siRNA-mediated SRF knockdown decreased F-actin formation and impaired EC migration and the formation of tube-like structures in vitro (Figure 7). Using the aortic ring assay, we demonstrated that mosaic deletion of SRF in ECs of S^f/S^f mice, induced by the adenovirus Cre-GFP, impaired the migration and elongation of vessel sprouts (Figure 6). Altogether, our results suggest that SRF is required for proper vessel migration. Interestingly, the angiogenic phenotype of the SRF^{ECKO} embryos is somewhat reminiscent of *Drosophila* bearing a mutation in the *Dsrf*, also known as *blistered* or *pruned*, expressed in tracheal tip cells (Guillemin et al., 1996). The formation of the ramified tracheal respiratory system of *Drosophila* shares some similarities with the vertebrate vascular system. Mutation of the *Dsrf* gene or *DMRTF*, which encodes a SRF cofactor activated by actin polymerization, reduces the branching and extension of terminal branches of the tracheal system (Guillemin et al., 1996; Somogyi and Rørth, 2004). Furthermore, this phenomenon is directly dependent on the hypoxia of surrounding tissues, which promotes the tracheal terminal branching via the FGF-FGFR-SRF-MRTF pathway (Centanin et al., 2008).

Moreover, previous studies have shown that SRF inactivation in different tissues, including heart, smooth muscle, and

(D–G) Confocal images of VE-cadherin (gray), phalloidin (red), and SRF (green) immunolabeling of (D and E) nonstimulated and (F and G) VEGF-stimulated HDMEC cells. (E and G) Knockdown of SRF with siSRF decreased F-actin and VE-cadherin staining compared to (D and F) control cells treated with siControl. VEGF increased the formation of stress fibers in the control cells, but not in SRF-deficient cells. Inserts show the cell nucleus revealed by the DAPI staining in (D)–(G). The scale bars are 20 μm in (D)–(F).

(H–K) Monolayer scratch wound healing assay in HDMECs treated with either (H and I) scrambled siRNA or (J and K) *Srf* siRNA.

(L) Quantification of cell migration in the wound healing assay. The error bars represent SEM; N = 6. ***p < 0.001.

(M–P) In vitro angiogenesis assay on Matrigel with HDMECs in (M) 0.5% SVF medium or (N–P) VEGF165 (50 ng/ml)-supplemented medium. (N) Cells treated with scrambled siRNA. (O) A mixture (1:1) of scrambled siRNA or *Srf* siRNA-treated cells. (P) *Srf* siRNA-treated cells.

(Q) Quantification of in vitro angiogenesis. Control cells did not rescue the capacity of SRF-deficient cells to form the tube-like structure.

The error bars represent SEM; N = 4. *p < 0.05; ***p < 0.001.

neurons, not only affects actin expression levels, but also actin filament treadmilling (Parlakian et al., 2005; Mericskay et al., 2007; Knöll et al., 2006). The actin cytoskeleton constantly remodels in migrating ECs, forming different structures, including filopodia, lamellipodia, and stress fibers (Lamalice et al., 2007). Actin treadmilling is actively regulated by small GTPases of the RhoA family that control the organization of actin during cell migration and play an important role downstream of VEGFR2 activation by VEGF (Lamalice et al., 2004; Ridley, 2006). Indeed, cell locomotion depends on RhoA-stimulated actomyosin contraction at the rear part of the cell (Pollard, 2003). Interestingly, RhoA has been shown to play a major role in SRF activation of the *β-actin* promoter (Sotiropoulos et al., 1999). Therefore, the impaired tip cell migration observed in SRF^{ECKO} embryos could be related to a deficient contractile apparatus. Interestingly, we have shown that VEGF promotes SRF expression in cultured ECs, and that this induction depends on the presence of CArG boxes in the SRF promoter region (Figure 7; Figure S4). This is in agreement with an earlier study, carried out by Tarnawski's group, demonstrating that SRF is activated by VEGF through both RhoA and MEK/ERK signaling pathways (Chai et al., 2004). In addition, we have shown that SRF is also important for VE-cadherin expression (Figures 5–7; Figures S2 and S5). VE-cadherin also plays an important role in mediating VEGF-VEGFR2 signaling (Lampugnani and Dejana, 2007; Vestweber, 2008), and its downregulation in the capillaries of SRF^{ECKO} embryos may also impair the VEGF response in ECs. It is of interest to note that VEGF is highly induced by regional hypoxia, and this pathway represents one of the major forces promoting angiogenesis throughout the embryo (Shweiki et al., 1992). Thus, SRF could be an important mediator in hypoxia-induced angiogenesis in the mouse, as in the tracheal terminal branching of *Drosophila*.

The vascular and neural systems share several molecular pathways involved in sprouting selection, guiding, and cell migration, including VEGF and Eph-ephrin signaling (Eichmann et al., 2005). Targeted inactivation of SRF in neurons was shown to impede neurite outgrowth and guidance mediated by EphA repulsive signals, as well as to downregulate *EphA4* and *EphA7* genes (Knöll et al., 2006). More recently, Ginty's group has shown that SRF is a major effector of both MEK/ERK and MAL signaling by NGF and is a key mediator of NGF-dependent target innervation by embryonic sensory neurons (Wickramasinghe et al., 2008). Interestingly, we observed a downregulation of the genes encoding the angiogenic guidance molecule ephrin-B2 and EphB4 receptor in the limb buds of SRF^{ECKO} embryos, which could be implicated in impaired vessel pathfinding in SRF^{ECKO}.

Dilatation of Capillaries in the SRF^{ECKO} Embryo

In addition to the tip cell defect, the vessel sprouts displayed a ballooned morphology with an accumulation of flattened ECs behind the tip cells (Figure 6; Figure S3). A similar distension of vessel tips has been observed in the hindbrains of embryos lacking heparin-binding VEGFA (Ruhrberg et al., 2002), reinforcing the idea that SRF is an important mediator of VEGF signaling. Interestingly, the sites of dilatation were not randomly distributed, but were instead found preferentially at the tip of the tail, in the marginal vein of the limb bud, and in the neural and perineural tissue (Figures 2 and 4), at least at the early stages of embryonic development. These peripheric regions, where the arterial and venous vessels make connections, may be the sites of more intense hemodynamic stress. These connections are defective in the SRF^{ECKO} mutant due to the deficient sprouting angiogenesis. In addition, the decreased vascular branching may enhance hemodynamic stress that would contribute to the appearance of more severe vascular defects, such as hemorrhages and aneurysms. Movies focused on the marginal vein of limb buds showed an altered blood flow in this region, in agreement with the additional hemodynamic burden hypothesis (Movies S1–S4). Similarly, our detailed analysis of the tail and neural capillary sprouts agrees with the hypothesis that a weakened cytoskeleton in the SRF-deficient stalk ECs may impair their resistance to increased hemodynamic stress.

The recruitment of vascular mural cells, pericytes (PC), and vascular SMCs (vSMC) is an important step toward vessel stabilization. PDGF-B and its receptor play an important role in vSMC/PC cell recruitment and proliferation during vascular growth, as well as in the TGF-β pathway. In addition, PDGF-B- and PDGFRβ-deficient mice developed numerous capillary microaneurysms that ruptured at late gestation (Hellström et al., 1999). We observed a significant downregulation of these two genes in the SRF^{ECKO} embryo, suggesting that a defect in recruitment of mural cells could be implicated in the phenotype of mutant embryos. However, whole-mount staining of neural capillaries for NG2, a PC-specific marker, and for smooth muscle α-actin, a vSMC marker, showed no major differences in PC or vSMC coverage of the vasculature between control and SRF^{ECKO} embryos, arguing against defective mural cell recruitment as a cause in this phenotype (Figure S6; Movies S13 and S14).

Altered Endothelial Cell-Cell Junctions in the SRF^{ECKO} Embryo

In parallel to the decreased expression of the *β-actin* gene, the deletion of *Srf* in ECs resulted in the decreased expression of genes implicated in transcription and integrin signaling, as well as those encoding cytoskeletal proteins, junction proteins, and growth factors and their receptors. Among the affected genes, we identified 12 new potential SRF target genes that have never before, to our knowledge, been described. Results from our quantitative RT-PCR, ChIP experiments, and luciferase reporter analysis suggest the potential direct regulation of some EC-specific genes such as *VE-cadherin*, *Alk1*, *Alk5*, and *endoglin* by SRF (Figure 5; Figure S2; data not shown). Analysis of the junction proteins VE-cadherin and ZO-1 revealed a disorganized pattern and a decreased protein expression in SRF^{ECKO} embryos. Electron microscopy analysis revealed the severe alteration of junctional complexes that link ECs together, in capillaries (Figure 6). Our results demonstrate that VE-cadherin, a major endothelial-specific adhesion molecule controlling cellular junctions and blood vessel formation (Vestweber, 2008), is a SRF target. The decreased VE-cadherin expression and its disorganization could influence not only the capillary integrity, but also sprouting angiogenesis. Recently, Affolter's group demonstrated the presence of "dot-like" and short "line-like" ZO-1- and VE-cadherin-containing structures in the migrating tip cells during intersegmental vessel formation of zebrafish embryos. These tip cells first contact each other and establish a VE-cadherin-containing interface that is then enlarged such that adjacent tip cells make extensive

contacts (Blum et al., 2008). This mechanism plays an important role in anastomosis and suggests that anastomosis defects may also be responsible for the vascular defects observed in the SRF^{ECKO} embryos. Interestingly, two other genes, *Alk1* and *endoglin*, mediating the TGF-β pathway, and with known involvement in hemorrhagic telangiactasia disease (HHT) type 1 and type 2, respectively, were also downregulated in mutant embryos (McAllister et al., 1994; Johnson et al., 1996). These endothelial junctional and signaling defects, in addition to the impaired cytoskeleton, likely contribute to the defect in the ERK phosphorylation observed in the SRF-deficient ECs (Figure 7) and to the appearance of hemorrhages and aneurysms observed in SRF^{ECKO} embryos (Figures 2 and 4). Taken together, our data have shown that SRF is important for the correct formation of cellular junctions in ECs. SRF inactivation leads to the weakening of the EC junctions and, consequently, to the destabilization of vessel cytoarchitecture, ultimately leading to hemorrhage and aneurysm.

In conclusion, we have demonstrated here that SRF plays an essential role in the endothelium, particularly in sprouting angiogenesis. Taking together our results and the current knowledge within this field, we propose the schematic model of SRF function in ECs during angiogenesis depicted in Figure S7. In response to angiogenic signals such as VEGF and FGF, SRF expression and activity in ECs is induced via both RhoA and MEK/ERK signaling pathways. SRF then increases not only the expression of its EC target genes, such as *β-actin* and *VE-cadherin*, but also enhances F-actin formation. In this way, SRF favors vessel stability and EC migration, promoting normal angiogenesis. SRF inactivation in ECs leads to a decreased expression of genes involved in EC function, including VE-cadherin and β-actin. The misexpression of such proteins could impair RhoA- and MEK/ERK-dependent biological functions in ECs. Consequently, SRF inactivation in ECs impairs the response to angiogenic signals, migration, and the integrity of cellular junctions of ECs, ultimately inducing malformations of the vascular network characterized by reduced capillary density, aneurysms, and hemorrhages. It is reasonable to assume that SRF is an important transcription factor in ECs, functioning downstream of VEGF signaling and/or other pathways such as FGF, to promote cytoskeleton and junctional reorganization, which are important for cell rearrangement, locomotion, and vessel integrity.

EXPERIMENTAL PROCEDURES

Targeting Inactivation of the *Srf* Gene in Embryonic Endothelial Cells

Intercross of the previously described SRF-floxed (S^f/S^f) and Tie1-Cre transgenic mice (Parlakian et al., 2004; Gustafsson et al., 2001) gave rise to double transgenic mice ($S^f/+$:Tie1-Cre). The $S^f/+$:Tie1-Cre male mice and the S^f/S^f female mice were then crossed to obtain S^f/S^f :Tie1-Cre mutant embryos. Genotyping of the mice and floxed *Srf* allele excision were performed by PCR as described previously (Parlakian et al., 2004). ROSA26 Cre reporter mice and Vim-LacZ transgenic mice have both been described previously (Soriano, 1999; Colucci-Guyon et al., 1994). This study conformed to institutional guidelines for the use of animals in research.

Histological Analysis, X-Gal Staining, and Immunohistochemistry

All embryos were staged as day 0.5 by the presence of a vaginal plug. These experiments were performed as described previously (Parlakian et al., 2004) and in Supplemental Data.

Quantification and Statistical Analysis

In tip cell quantification, we blind-scored tip cells as previously described (Hellström et al., 2007). We used ten fields sized 455 × 455 μm per hindbrain and six hindbrains/group (SRF^{ECKO} and control). In filopodia protrusion quantification, we scored the filopodia bursts from 12 tip cells for each hindbrain (6 hindbrains/group). Branching point measurements were counted in 20 confocal fields sized 455 × 455 μm in 6 hindbrains/group or 4 limb buds/group. For branching point measurements of the intersomitic region, we scored branching points in six intersomitic regions, in the eight limb buds from four anti-PECAM1, whole-mount, immunolabeled embryos and four X-gal-stained embryos. All quantitative data were analyzed by using Fisher post hoc tests for repeated measures and Student's unpaired t tests for comparison with control mice at specific times. The data shown are means ± SEM. p values < 0.05 were considered statistically significant.

Electron Microscopy

Tissue samples from limb buds were fixed in solution containing 2% paraformaldehyde, 1.5% glutaraldehyde, and 0.1 M phosphate buffer; postfixed for 1 hr at 4°C with 2% osmium tetroxide and 2% uranyl acetate solution; dehydrated in a series of alcohol; and embedded in epoxy resin. Sections were viewed by transmission electron microscopy.

Quantitative RT-PCR Assay

Forelimbs, heads, and dorsal sections were collected from fresh-harvested embryos at different time points. After genotyping, total RNA was extracted from each embryonic sample by using the MicroRNA kit (QIAGEN). The first-strand cDNA synthesis and PCR analysis were performed as previously described (Parlakian et al., 2005). Primer sequences are listed in Supplemental Data.

Western Blot Analysis

Western blot analysis was performed as described previously (Parlakian et al., 2005) by using the following different antibodies: SRF (1:200), ZO1 (1:200), VE-cadherin (1:200, BD Bioscience; 1:250, BV9, Santa Cruz), connexin43 (1:400, BD Bioscience), VEGFR2 (1:500, Cell Signaling), β-actin (1:400, Sigma), ERK1/2, p-ERK1/2 (Thr202/204) (1:1000, Cell Signaling), and anti-GAPDH (1:400, Santa Cruz).

Aortic Ring Assay

C57/BL6 S^f/S^f mice were euthanized, and thoracic aortic rings (1 mm) were isolated and incubated in MCDB131 medium with 10% FBS for 16 hr in the presence of either adenovirus Cre-GFP or GFP and were then embedded in growth factor-reduced Matrigel (BD Bioscience) overlaid with MCDB131 medium supplemented with 2 mM Glutamax (Invitrogen), 10 U/ml heparin, 100 U/ml penicillin, 100 μg/ml streptomycin, 10% FBS, and VEGF (50 ng/ml). Microvessel outgrowth was visualized by microscopy at different time points.

Matrigel Angiogenesis Assays

Primary human dermal microvascular ECs ([HDMECs], purchased from Promocell), transfected with scrambled siRNA or anti-*Srf* siRNA, were plated in 24-well plates, precoated with 300 μl growth factor-reduced Matrigel (BD Bioscience), at 50,000 cells/well. Cells were cultured in MCDB131 medium supplemented with 2 mM Glutamax (Invitrogen), 10 U/mL heparin, 100 U/mL penicillin, 100 μg/mL streptomycin, and 0.5% SVF. Additionally, cells were stimulated with VEGF (50 ng/ml) or bFGF (50 ng/ml). A total of 16 hr after seeding, photographs of representative 10× fields were taken and the lengths of the endothelial tubes were measured.

Wound Healing Assay

Primary HDMECs, transfected with scrambled siRNA or anti-*Srf* siRNA, were plated in 12-well plates at 50,000 cells/cm^2 and were allowed to grow until confluence. The wound was created by using a pipette cone. Then, cells were washed once with culture medium and were allowed to migrate in DMEM/0.5% FBS. The wounded area was monitored over the course of 24 hr, and micrographs were taken every 4 hr.

Growth Factor Simulation Assay

Primary HDMECs and HuBMEC lines were plated in 12-well or 6-well plates at 50,000 cells/cm^2 and were cultured in EC growth medium MV2 (Promocell)

over the course of 24 hr. Afterward, the medium was replaced with DMEM/0.5% FBS overnight, and cells were then left untreated or stimulated with VEGF (50 ng/ml) or bFGF (50 ng/ml). Protein samples were extracted with Kinexus buffer, and mRNA was extracted with Trizol reagent (Invitrogen) as indicated by the manufacturer's protocol.

SUPPLEMENTAL DATA

Supplemental Data include Experimental Procedures, a table, figures, and movies and can be found with this article online at http://www.developmentalcell.com/cgi/content/full/15/3/448/DC1/.

ACKNOWLEDGMENTS

C.A.F. was supported by the Fondation pour la Recherche Medicale. We thank A. Eichmann, D. Daegelen, D. Tuil, A. Janin, A. Grosfeld, and S. Germain for fruitful discussion and suggestions; B. el-Zhalek for assistance with electronic microscope analysis; and C. Freitas and E. Gomez for their generous gift of antibodies. This work was supported by l'Agence Nationale pour la Recherche (COD2005), La Fondation de France, and Association Française contre les Myopathies.

Received: March 17, 2008
Revised: June 25, 2008
Accepted: July 31, 2008
Published: September 15, 2008

REFERENCES

Adams, R.H., and Alitalo, K. (2007). Molecular regulation of angiogenesis and lymphangiogenesis. Nat. Rev. Mol. Cell Biol. *8*, 464–478.

Arsenian, S., Weinhold, B., Oelgeschläger, M., Rüther, U., and Nordheim, A. (1998). Serum response factor is essential for mesoderm formation during mouse embryogenesis. EMBO J. *17*, 6289–6299.

Blum, Y., Belting, H.G., Ellertsdottir, E., Herwig, L., Lüders, F., and Affolter, M. (2008). Complex cell rearrangements during intersegmental vessel sprouting and vessel fusion in the zebrafish embryo. Dev. Biol. *316*, 312–322. Published online February 13, 2008. doi: 10.1016/j.ydbio.2008.01.038.

Carmeliet, P. (2005). Angiogenesis in life, disease and medicine. Nature *438*, 932–936.

Centanin, L., Dekanty, A., Romero, N., Irisarri, M., Gorr, T.A., and Wappner, P. (2008). Cell autonomy of HIF effects in *Drosophila*: tracheal cells sense hypoxia and induce terminal branch sprouting. Dev. Cell *14*, 547–558.

Chai, J., and Tarnawski, A.S. (2002). Serum response factor: discovery, biochemistry, biological roles and implications for tissue injury healing. J. Physiol. Pharmacol. *53*, 147–157.

Chai, J., Jones, M.K., and Tarnawski, A.S. (2004). Serum response factor is a critical requirement for VEGF signalling in endothelial cells and VEGF-induced angiogenesis. FASEB J. *18*, 1264–1266.

Colucci-Guyon, E., Portier, M.M., Dunia, I., Paulin, D., Pournin, S., and Babinet, C. (1994). Mice lacking vimentin develop and reproduce without an obvious phenotype. Cell *79*, 679–694.

Dejana, E., Taddei, A., and Randi, A.M. (2007). Foxs and Ets in the transcriptional regulation of endothelial cell differentiation and angiogenesis. Biochim. Biophys. Acta *1775*, 298–312.

Eichmann, A., Makinen, T., and Alitalo, K. (2005). Neural guidance molecules regulate vascular remodeling and vessel navigation. Genes Dev. *19*, 1013–1021.

Gerhardt, H., Golding, M., Fruttiger, M., Ruhrberg, C., Lundkvist, A., Abramsson, A., Jeltsch, M., Mitchell, C., Alitalo, K., Shima, D., and Betsholtz, C. (2003). VEGF guides angiogenic sprouting utilizing endothelial tip cell filopodia. J. Cell Biol. *161*, 1163–1177. Published online June 16, 2003. doi: 10.1083/jcb.200302047.

Gridley, T. (2007). Notch signaling in vascular development and physiology. Development *134*, 2709–2718. Published online July 4, 2007. doi: 10.1242/dev.004184.

Guillemin, K., Groppe, J., Ducker, K., Treisman, R., Hafen, E., Affolter, M., and Krasnow, M.A. (1996). The pruned gene encodes the *Drosophila* serum response factor and regulates cytoplasmic outgrowth during terminal branching of the tracheal system. Development *122*, 1353–1362.

Gustafsson, E., Brakebusch, C., Hietanen, K., and Fässler, R. (2001). Tie-1-directed expression of Cre recombinase in endothelial cells of embryoid bodies and transgenic mice. J. Cell Sci. *114*, 671–676.

Hanahan, D., and Folkman, J. (1996). Patterns and emerging mechanisms of the angiogenic switch during tumorigenesis. Cell *86*, 353–364.

Hellström, M., Kalén, M., Lindahl, P., Abramsson, A., and Betsholtz, C. (1999). Role of PDGF-B and PDGFR-β in recruitment of vascular smooth muscle cells and pericytes during embryonic blood vessel formation in the mouse. Development *126*, 3047–3055.

Hellström, M., Phng, L.K., Hofmann, J.J., Wallgard, E., Coultas, L., Lindblom, P., Alva, J., Nilsson, A.K., Karlsson, L., Gaiano, N., et al. (2007). Dll4 signalling through Notch1 regulates formation of tip cells during angiogenesis. Nature *445*, 776–780. doi: 10.1038/nature05571.

Johnson, D.W., Berg, J.N., Baldwin, M.A., Gallione, C.J., Marondel, I., Yoon, S.J., Stenzel, T.T., Speer, M., Pericak-Vance, M.A., Diamond, A., et al. (1996). Mutations in the activin receptor-like kinase 1 gene in hereditary haemorrhagic telangiectasia type 2. Nat. Genet. *13*, 189–195.

Knöll, B., Kretz, O., Fiedler, C., Alberti, S., Schütz, G., Frotscher, M., and Nordheim, A. (2006). Serum response factor controls neuronal circuit assembly in the hippocampus. Nat. Neurosci. *9*, 195–204. Published online January 15, 2006. doi: 10.1038/nn1627.

Lamalice, L., Houle, F., Jourdan, G., and Huot, J. (2004). Phosphorylation of tyrosine 1214 on VEGFR2 is required for VEGF-induced activation of Cdc42 upstream of SAPK2/p38. Oncogene *23*, 434–445.

Lamalice, L., Le Boeuf, F., and Huot, J. (2007). Endothelial cell migration during angiogenesis. Circ. Res. *100*, 782–794.

Lampugnani, M.G., and Dejana, E. (2007). Adherens junctions in endothelial cells regulate vessel maintenance and angiogenesis. Thromb. Res. *120* (*Suppl 2*), S1–S6.

McAllister, K.A., Grogg, K.M., Johnson, D.W., Gallione, C.J., Baldwin, M.A., Jackson, C.E., Helmbold, E.A., Markel, D.S., McKinnon, W.C., Murrell, J., et al. (1994). Endoglin, a TGF-β binding protein of endothelial cells, is the gene for hereditary haemorrhagic telangiectasia type 1. Nat. Genet. *8*, 345–351.

Mericskay, M., Blanc, J., Tritsch, E., Moriez, R., Aubert, P., Neunlist, M., Feil, R., and Li, Z. (2007). Inducible mouse model of chronic intestinal pseudo-obstruction by smooth muscle-specific inactivation of the SRF gene. Gastroenterology *133*, 1960–1970. Published online September 16, 2007. doi: 10.1053/j.gastro.2007.09.010.

Miano, J.M. (2003). Serum response factor: toggling between disparate programs of gene expression. J. Mol. Cell. Cardiol. *35*, 577–593.

Miano, J.M., Ramanan, N., Georger, M.A., de Mesy Bentley, K.L., Emerson, R.L., Balza, R.O., Jr., Xiao, Q., Weiler, H., Ginty, D.D., and Misra, R.P. (2004). Restricted inactivation of serum response factor to the cardiovascular system. Proc. Natl. Acad. Sci. USA *101*, 17132–17137. Published online November 29, 2004. doi: 10.1073/pnas.0406041101.

Niu, Z., Yu, W., Zhang, S.X., Barron, M., Belaguli, N.S., Schneider, M.D., Parmacek, M., Nordheim, A., and Schwartz, R.J. (2005). Conditional mutagenesis of the murine serum response factor gene blocks cardiogenesis and the transcription of downstream gene targets. J. Biol. Chem. *280*, 32531–32538. Published online May 31, 2005. doi: 10.1074/jbc.M501372200.

Parlakian, A., Tuil, D., Hamard, G., Tavernier, G., Hentzen, D., Concordet, J.P., Paulin, D., Li, Z., and Daegelen, D. (2004). Targeted inactivation of serum response factor in the developing heart results in myocardial defects and embryonic lethality. Mol. Cell. Biol. *24*, 5281–5289.

Parlakian, A., Charvet, C., Escoubet, B., Mericskay, M., Molkentin, J.D., Gary-Bobo, G., De Windt, L.J., Ludosky, M.A., Paulin, D., Daegelen, D., et al. (2005). Temporally controlled onset of dilated cardiomyopathy through disruption of the SRF gene in adult heart. Circulation *112*, 2930–2939.

Pollard, T.D. (2003). The cytoskeleton, cellular motility and the reductionist agenda. Nature *422*, 741–745.

Ridley, A.J. (2006). Rho GTPases and actin dynamics in membrane protrusions and vesicle trafficking. Trends Cell Biol. *16*, 522–529. Published online September 1, 2006. doi: 10.1016/j.tcb.2006.08.006.

Risau, W. (1997). Mechanisms of angiogenesis. Nature *386*, 671–674.

Roca, C., and Adams, R.H. (2007). Regulation of vascular morphogenesis by Notch signaling. Genes Dev. *21*, 2511–2524.

Ruhrberg, C., Gerhardt, H., Golding, M., Watson, R., Ioannidou, S., Fujisawa, H., Betsholtz, C., and Shima, D.T. (2002). Spatially restricted patterning cues provided by heparin-binding VEGF-A control blood vessel branching morphogenesis. Genes Dev. *16*, 2684–2698.

Shweiki, D., Itin, A., Soffer, D., and Keshet, E. (1992). Vascular endothelial growth factor induced by hypoxia may mediate hypoxia-initiated angiogenesis. Nature *359*, 843–845.

Somogyi, K., and Rørth, P. (2004). Evidence for tension-based regulation of *Drosophila* MAL and SRF during invasive cell migration. Dev. Cell *7*, 85–93.

Soriano, P. (1999). Generalized lacZ expression with the ROSA26 Cre reporter strain. Nat. Genet. *21*, 70–71.

Sotiropoulos, A., Gineitis, D., Copeland, J., and Treisman, R. (1999). Signal-regulated activation of serum response factor is mediated by changes in actin dynamics. Cell *98*, 159–169.

Suchting, S., Freitas, C., le Noble, F., Benedito, R., Bréant, C., Duarte, A., and Eichmann, A. (2007). The Notch ligand Delta-like 4 negatively regulates endothelial tip cell formation and vessel branching. Proc. Natl. Acad. Sci. USA *104*, 3225–3230. Published online February 12, 2007. doi: 10.1073/pnas.0611177104.

Sun, Q., Chen, G., Streb, J.W., Long, X., Yang, Y., Stoeckert, C.J., Jr., and Miano, J.M. (2006). Defining the mammalian CArGome. Genome Res. *16*, 197–207. Published online December 19, 2005.

Torres-Vázquez, J., Gitler, A.D., Fraser, S.D., Berk, J.D., Pham, V.N., Fishman, M.C., Childs, S., Epstein, J.A., and Weinstein, B.M. (2004). Semaphorin-plexin signaling guides patterning of the developing vasculature. Dev. Cell *7*, 117–123.

Treisman, R. (1987). Identification and purification of a polypeptide that binds to the c-fos serum response element. EMBO J. *6*, 2711–2717.

Vestweber, D. (2008). VE-cadherin: the major endothelial adhesion molecule controlling cellular junctions and blood vessel formation. Arterioscler. Thromb. Vasc. Biol. *28*, 223–232. Published online December 27, 2007. doi: 10.1161/ATVBAHA.107.158014.

Wickramasinghe, S.R., Alvania, R.S., Ramanan, N., Wood, J.N., Mandai, K., and Ginty, D.D. (2008). Serum response factor mediates NGF-dependent target innervation by embryonic DRG sensory neurons. Neuron *58*, 532–545.